Surface & Coatings Technology 395 (2020) 125691

Contents lists available at ScienceDirect

Surface & Coatings Technology

journal homepage: www.elsevier.com/locate/surfcoat

Plasma-ion-assisted deposition of HfO_2 films with low UV absorption

Wenyuan Deng*, Chunshui Jin, Chun Li, Shun Yao, Bo Yu, Yu Liu

State Key Laboratory of Applied Optics, Changchun Institute of Optics, Fine Mechanics and Physics, Chinese Academy of Sciences, Changchun, Jilin 130033, China

ARTICLE INFO

Keywords:
HfO_2
Thin film
Optical properties
Microstructure
PIAD-EBE

ABSTRACT

HfO_2 films were fabricated by plasma-ion-assisted deposition of electron beam evaporation (PIAD-EBE) for low absorption applications in UV. The optical, structural and composition properties of the deposited HfO_2 films were systematically investigated to evaluate the influence and its mechanism of four kind process parameters. The results revealed that the crystal orientation of the monoclinic phase in the HfO_2 films was very sensitive to momentum transfer originating from the plasma ions or the substrate temperature. Besides, the evolution of the crystal orientation with momentum transfer showed a strong correlation with the refractive index and its inhomogeneity in the HfO_2 films. An optimized HfO_2 film with very low extinction coefficients and high refractive index, which was critical to UV applications such as HR mirrors and solar-blind filters, was obtained.

1. Introduction

In the last decade, UV laser sources, such as excimer lasers and storage ring free-electron lasers, have developed rapidly [1–3]. The application of these laser sources creates challenges regarding the performance of the optical interference coatings used in UV laser sources [2,3]. In contrast to visible or near IR lasers, the main reason for the damage of the optical interference coatings in UV lasers is the absorption, which mainly arises from the high-index materials. In addition to the resistance against laser damage, low absorption was also critical to obtain high spectrum performance of UV HR and other UV applications, such as solar-blind detection [4–5]. Due to its relatively high refractive index in the UV region, HfO_2 has been one of the few available and the most important high-index oxide films for laser applications in the UV region down to 230 nm [3,6–7]. Actually, due to the good optical properties from the IR to UV range [8–12], thermal and chemical stability [14–16], higher laser resistance [16–20], and high-k gate dielectrics [21–25]. Numerous studies have been devoted to the fabrication and characterization of HfO_2 films deposited by different techniques, including electron beam evaporation without (EBE) [15,16,26,27] and with energy assistance (Ion-assisted deposition and plasma-ion-assisted deposition) [13,15,27–32], ion plating [33], ion beam sputtering [34,35], and magnetron sputtering [36–38]. Plasma-ion-assisted deposition (PIAD) can fabricate denser film than EBE and provide significant potential in the tuning of film properties such as humidity stability, stress, mechanical durability, and the material refractive index. This tunability was realized by controlling process parameters such as bias voltage, beam current, working gas and gas flow rate [14,28,31,32]. However, the use of ion assistance may also shift the absorption edge of the deposited film to longer wavelengths, resulting in higher intrinsic absorption and a decreased LIDT [20,27,28,40]. At the same time, it is known that the structural and optical properties of HfO_2 films are very sensitive to the above variables and other deposition conditions, such as substrate temperature and oxygen partial pressure [6,28–32,39,43,45,46]. Therefore, although there have been many reports about the UV properties of HfO_2 films deposited by PIAD, the reported absorption results have not very been satisfying, especially for wavelengths ranging from 220 nm to 250 nm [4,15,18,27,31,32,44]. Considering the numerous process parameters involved in PIAD and the continually increasing requirements low UV absorption to HfO_2 coatings, more detailed studies of the correlation between the process parameters and properties of HfO_2 films deposited by PIAD are necessary to achieve denser structure and lower UV absorption desired for UV laser applications [3,31].

In this work, HfO_2 films were fabricated by PIAD using different combinations of four process parameters (bias voltages of the Advanced Plasma Source (APS), substrate temperature, oxygen flow rate in the chamber and oxygen flow rate in the APS). The optical and structural properties of the fabricated HfO_2 films, including the optical constant, absorption, spectral shift, crystallinity, surface morphology, O/Hf atomic ratio, and SEM cross-section, were systematically characterized. The specific influences of different process parameters on the properties of the HfO_2 films were evaluated in detail by investigating the correlation between the optical and structural properties of samples deposited with different process parameters.

* Corresponding author.
E-mail address: dengwy@ciomp.ac.cn (W. Deng).

https://doi.org/10.1016/j.surfcoat.2020.125691
Received 23 May 2019; Received in revised form 29 February 2020; Accepted 24 March 2020
Available online 13 May 2020

Table 1
Main deposition parameters and characterization methods.

Sample	Bias voltage (V)	Substrate temperature (°C)	O_2 flow rate in chamber (sccm)	O_2 flow rate in APS (sccm)	Non-optical analytics
S1	90	200	30	25	XRD, AFM, SEM, EDX
S2	120	200	30	25	XRD, AFM, SEM, EDX
S3	150	200	30	25	XRD, AFM, SEM, EDX
S4	90	200	20	25	XRD, AFM, SEM, EDX
S5	120	200	20	25	XRD, AFM, SEM, EDX
S6	120	150	20	25	XRD, AFM, SEM, EDX
S7	120	250	20	25	XRD, AFM, SEM, EDX
S8	120	300	20	25	XRD, AFM, SEM, EDX
S9	120	200	20	20	XRD, AFM, SEM, EDX
S10	120	200	20	30	XRD, AFM, SEM, EDX

2. Experiments

2.1. Layer deposition

All samples were prepared by a Leybold Optics Syrus Pro deposition system (DUV 1110) equipped with a Leybold Optics Advanced Plasma Source (APS Pro). A lanthanum hexaboride cathode (LaB6) was used in the APS Pro due to its low defect density and high plasma current necessary for the densification of hafnia.

The deposition parameters in this study were summarized in Table 1. The four process parameters were the bias voltage of the APS source, substrate temperature, the O_2 flow rate in the chamber and O_2 flow rate in the APS source. According to the possible influences of the different parameters, comprehensive experiments involving 10 depositing runs have been performed. In addition to the process parameters, the non-optical characterization methods were also listed in Table 1.

For all the deposition runs, the film thickness was controlled by quartz monitoring, and the deposition rate was fixed to 0.3 nm/s. During all the deposition runs, base pressure inside the chamber before the deposition was below 10^{-6} mbar. In each deposition run, double-polished fused silica with 1 in. in diameter and 2 mm in thickness were coated for the optical measurements, and single-polished silicon was also coated for additional non-optical analytic (EDX and SEM).

2.2. Layer characterization

2.2.1. Optical constants

Transmission and reflection spectra in the wavelength range of 200–800 nm were measured using a Lambda 950 spectrophotometer equipped with a VN-measurement attachment for an absolute reflection measurement. From the measured transmission and reflection spectra, the film thickness-d and optical constants (refractive index n and extinction coefficients k) of samples deposited with different parameters can be obtained using the OptiChar module of the commercial software OptiLayer [41]. The optical band gap of HfO_2 is near 220 nm, which means that the dispersion relationship below 220 nm may be different from normal dispersion. In addition, HfO_2 films deposited by EBE always show bulk inhomogeneity in the refractive index [32,35,40,42]. For the above reasons, the precise reverse fitting of the transmission and reflection spectra from 200 nm to 800 nm was not easy to realize [42]. To obtain the exact refractive index and extinction coefficients of the different samples, which is important to evaluate the influence of different parameters, a two-step fitting strategy was adopted.

In the first step, transmission and reflection spectra in the wavelength range of 230–800 nm were reverse fitted to obtain the film thickness, refractive index, extinction coefficient, and the inhomogeneity of the refractive index in the same wavelength range. During this reversion, the refractive index of all samples was presented in the form [42]

$$n(z,\lambda) = q(z)n(\lambda) \tag{1}$$

where q(z) was the inhomogeneity factor describing film inhomogeneity and n(λ) was the mean refractive index of the inhomogeneous film. For comparability, it was assumed that all samples were slightly inhomogeneous. A linear refractive index profile model was used and q(z) can be expressed by the equation [42]

$$q(z) = 1 + \delta(z/d - 1/2) \tag{2}$$

where δ was the degree of inhomogeneity, defined as [41]

$$\delta = (n_0(\lambda) - n_1(\lambda))/n(\lambda) \times 100\% \tag{3}$$

where n_0 and n_1 were the refractive indices of the top and bottom surfaces, respectively. A standard three-parametric Cauchy model was adopted for the n(λ) and k(λ).

$$n(\lambda) = n_\infty + \frac{A}{\lambda^2} + \frac{B}{\lambda^4},\ k(\lambda) = B_0 \exp\left(-\frac{B_1}{\lambda} - B_2\lambda\right). \tag{4}$$

Then, by fixing the thickness and refractive index inhomogeneity, transmission and reflection spectra in the 200–250 nm range were reverse fitted to obtain the refractive index and extinction coefficients in the same wavelength range. A model that assumes arbitrary but smooth dependence of refractive index and extinction coefficient on wavelength was adopted in this reversion [41]. The refractive index and extinction coefficients in the entire wavelength range of 200–800 nm were obtained by combing the two wavelength range at the intersection of them. The relative error of n and d by the above method was believed to be below 1%.

2.2.2. Spectral shift

Evaporated films were tended to behavior a thermal and vacuum related spectral shift due to the porous structure. To quantify the spectral shift with time, the transmission spectrum of all samples was measured two times. The first measurement was performed immediately when the sample was taken out from the evaporation chamber. The second measurement was performed after storage in atmospheric room temperature conditions for three months. The spectral shift was defined with relative wavelength shift of transmission peak between the two measurements, namely defined as $(\lambda_1\text{-}\lambda_0)/\lambda_0 \times 100\%$, where λ_0 and λ_1 was the peak wavelength around 270 nm of the transmission spectrum in the first and second measurements.

2.2.3. SEM, AFM and XRD

To evaluate the surface topography and microstructure of HfO_2 film, all samples deposited on silicon substrate have been analyzed by Field-emission scanning electron microscopy (FE-SEM, S-4800, and HITACHI) to obtain high-resolution images of the cross-sectional and surface of HfO_2 film. In SEM measurement, the cross-section of the cleaved sample was measured by tilted with 45°. All samples deposited on the fused silica substrate were measured by a NanoSurf force microscope (AFM) with dynamic mode. In AFM measurement, 2 μm × 2 μm region is sampled with 256 × 256 points. The root mean square (RMS) surface roughness was obtained by the AFM software. In order to obtain crystalline information, grazing incidence X-ray diffractograms of HfO_2 samples deposited on fused silica substrate were

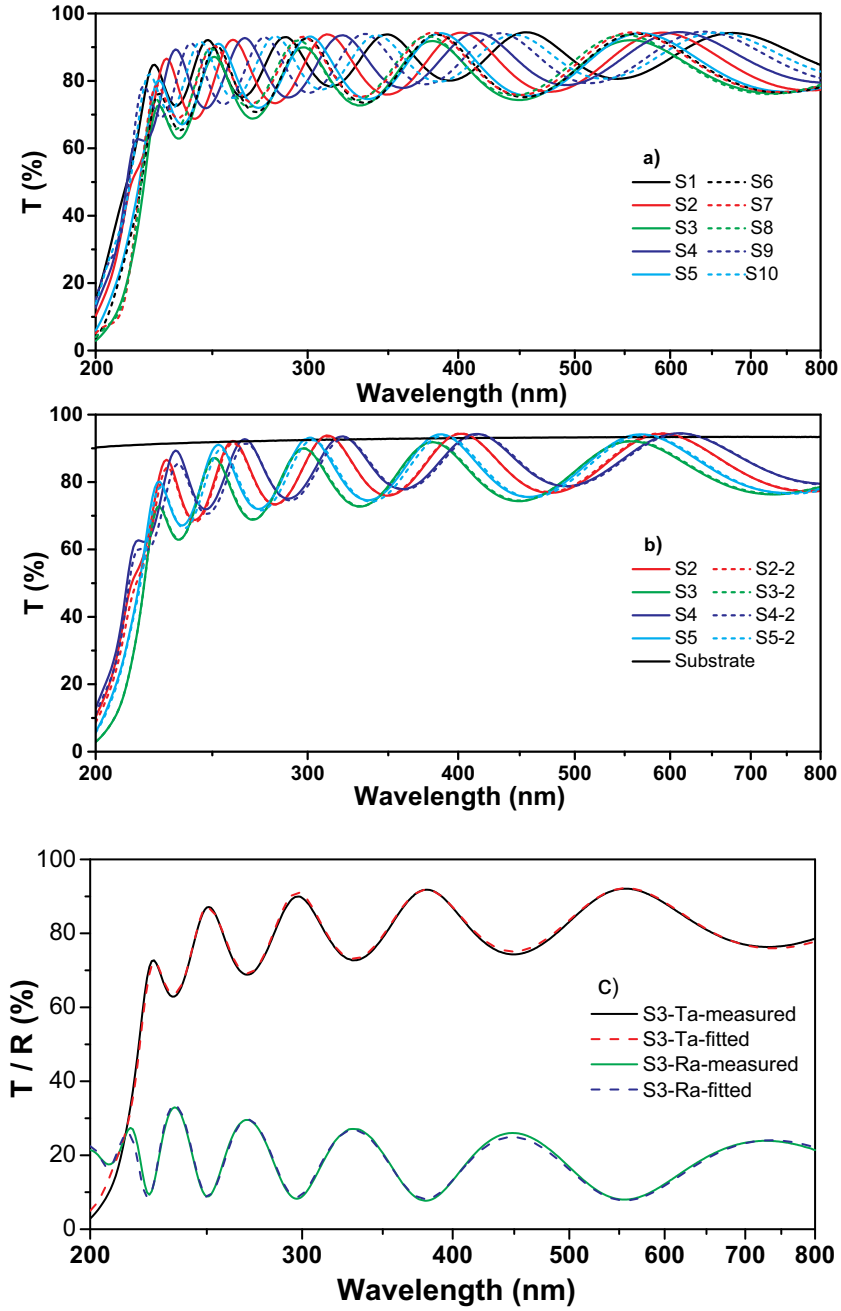

Fig. 1. a) Transmittance of all HfO_2 samples; b) transmittance of selected HfO_2 samples; c) measured and fitted spectra of samples S3 with the largest refractive index inhomogeneity.

measured by using a Bruker D8 Advance diffraction meter (nickel-filtered Cu Kα radiation, λ = 0.154178 nm, 40 kV, 40 mA) in the 2θ range of 20–60° with step size of 0.05°.

2.2.4. EDX

In order to obtain the composition of HfO_2 film, energy-dispersive X-ray spectroscopy (EDX, genesis 2000 EDAX) of all samples deposited on fused silica were measured with an accelerating voltage of 15 kV. To obtain the quantitative results of the Hf/O atomic ratio in the deposited HfO_2 films, an HfO_2 compound with a standard atomic ratio of 2 was used to calibrate the EDX instrument before measuring the HfO_2 films.

3. Results

3.1. Optical properties

The measured UV-VIS transmission spectra of all samples and the spectral shifts of selected samples were illustrated in Fig. 1a) and b), respectively. By comparing the transmission spectra of the HfO_2 samples with those of the fused silica substrate, it is obvious that many HfO_2 samples are inhomogeneous [42,47]. As stated in above Section 2.2.1, the exact refractive index and extinction coefficients of the different HfO_2 samples were very important to evaluate the influence of different parameters. As a proof, Fig. 1c) presented the experimental and fitted transmission/reflection spectra of the samples with the largest inhomogeneity of refractive index. The fitted transmission/reflection spectra agree well with the measured transmission/reflection

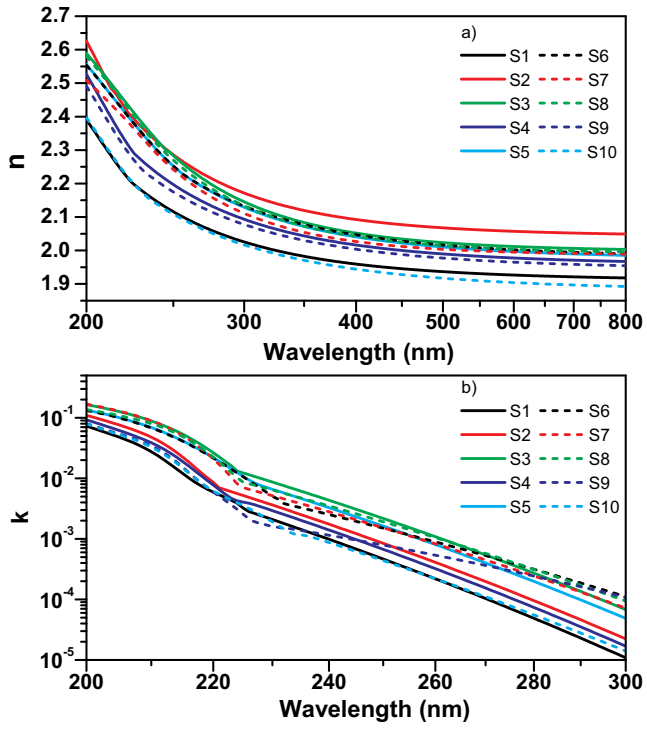

Fig. 2. Optical constants of the HfO_2 film: a) refractive index; b) extinction coefficients.

spectra, which indicated the relative errors in the inversion of transmission/reflection spectra was very low.

The obtained refractive index n and extinction coefficients k of all HfO_2 samples were depicted in Fig. 2a) and b), respectively. To cast a clearer picture of the properties of the different HfO_2 samples, the film thickness, refractive index and extinction coefficient at 250 nm, and the spectral shift, degree of refractive index inhomogeneity, and optical bandgap E04 (defined as the photon energy where the absorption coefficient $\alpha = 4\pi k/\lambda$ equals 10,000 cm^{-1}) are listed in Table 2. As shown in Table 2, one of the most impressive variations in the optical properties is the degree of refractive index inhomogeneity, which was directly caused by the microstructure of HfO_2 film. Among the four process parameters investigated in this paper, the APS bias voltage and substrate temperature have a significant influence on refractive index inhomogeneity of HfO_2 films.

3.2. Structure-related results

Fig. 3 displays the X-ray diffraction profiles of all HfO_2 samples deposited on the fused silica substrates. From Fig. 3, it can be seen that all HfO_2 samples have a nanocrystalline structure of the monoclinic phase. However, the diffraction peaks in the different samples significantly varied. For samples S3, S7, and S8, there are two strong diffraction peaks at approximately $2\theta = 28.3^\circ$ and $2\theta = 34.3^\circ$, corresponding to the (−111) and (002) crystal plane, respectively. However, the other samples have only two other diffraction peaks located at approximately $2\theta = 34.8^\circ$ and $2\theta = 38.9^\circ$, corresponding to the (020) and (021) crystal plane, respectively. For this reason, the crystalline phase was divided and marked only with the (−111) or (021) crystal plane in Table 2. To quantify the variation of crystal plane in different samples, the crystalline sizes of (002) crystal plane in samples S3, S7 and S8, and the crystalline sizes of (020) crystal plane in the other samples except for S5 were calculated by fitting the diffraction peaks of the corresponding plane. For sample S5, the crystalline size of (020) and (002) crystal plane were obtained by fitting the overlapping diffraction peaks of them.

Cross-sectional SEM can intuitively display the information of the size and arrangement of crystalline columnar in films, which is one of the most important structure-related characterizations. From Fig. 4, it can be seen that the size and arrangement of the crystalline columnar in different samples varied significantly. Among them, the cross-section of samples S3 was the most distinctive. It is obvious that the microstructure of sample S3 is not uniform in either the film growth direction or its vertical direction. In the film growth direction, it seems that sample S3 can be divided into three sublayers. Firstly, there is a thin transition sublayer near the substrate. The middle sublayer contained obviously the crystalline columnar structure. The top sublayer was very thin and seemed to have happened re-melting and condensation between adjacent deposited molecules. There is no layered structure along the direction of film growth and the boundary of the crystalline columnar structure was not very distinct for sample S1, S2, and S4. All the samples S5-S10 exhibited similar cross-sectional, which can be divided into a thin transition sublayer near the substrate and a top layer contained obviously the crystalline columnar structure.

The measured AFM images of all the HfO_2 samples were illustrated in Fig. 5, and the surface roughness were listed in Table 2. It can be seen that both the surface morphology and roughness varied significantly with specific process parameters. It should be noted that the surface morphology from AFM was amazing in agreement with that from SEM measurement.

3.3. EDX results

The obtained results of the Hf/O atomic ratio are listed in the last column of Table 2. The O/Hf atomic ratio varies from 1.7 to 2.0 in different samples. The O/Hf atomic ratios of sample S1 and sample S10 are close to the standard stoichiometric ratio of 2. The O/Hf atomic ratios of the other samples are lower than 2, indicating a loss of O atoms during the deposition of HfO_2. According to EDX scans, Ar content was detected in samples S3, S5, S7, and S8, while no Ar content was

Table 2
Survey of characterization results.

Sample	d (nm)	n@250 nm	Degree of inhomogeneity (%)	k@250 nm (10^{-3})	E_{04} (eV)	Spectrum shift (%)	Crystal phase	RMS roughness (nm)	Atom ratio (O/Hf)
Subs				Fused silica					Si
S1	361.0	2.057	−5.7	0.465	5.820	−0.30	(021)	1.53	1.974
S2	299.3	2.201	−7.8	0.847	5.730	0.13	(021)	1.57	1.885
S3	276.4	2.279	8.0	2.170	5.574	0.10	(−111)	0.88	1.743
S4	319.1	2.127	−6.6	0.672	5.752	0.26	(021)	2.14	1.871
S5	280.8	2.249	−4.4	1.620	5.596	0.41	(021)	3.18	1.792
S6	280.5	2.248	−3.9	1.500	5.598	0.62	(021)	3.90	1.793
S7	279.4	2.246	−6.8	1.520	5.615	0.37	(−111)	6.49	1.804
S8	274.3	2.270	0.0	1.920	5.603	0.43	(−111)	5.83	1.785
S9	337.7	2.101	−5.3	0.790	5.732	−0.61	(021)	6.70	1.858
S10	352.4	2.067	−4.0	0.438	5.788	−0.29	(021)	6.60	1.961

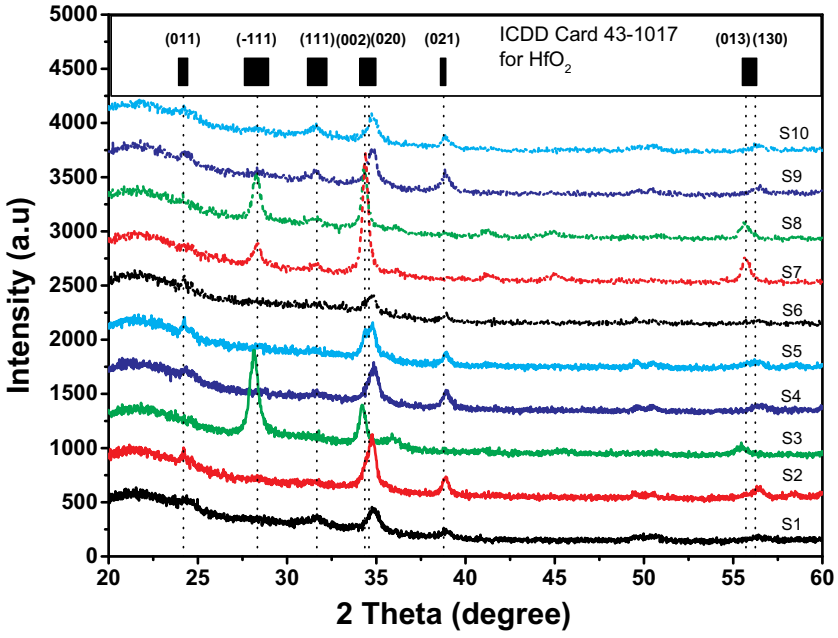

Fig. 3. X-ray diffraction curves of the HfO_2 samples.

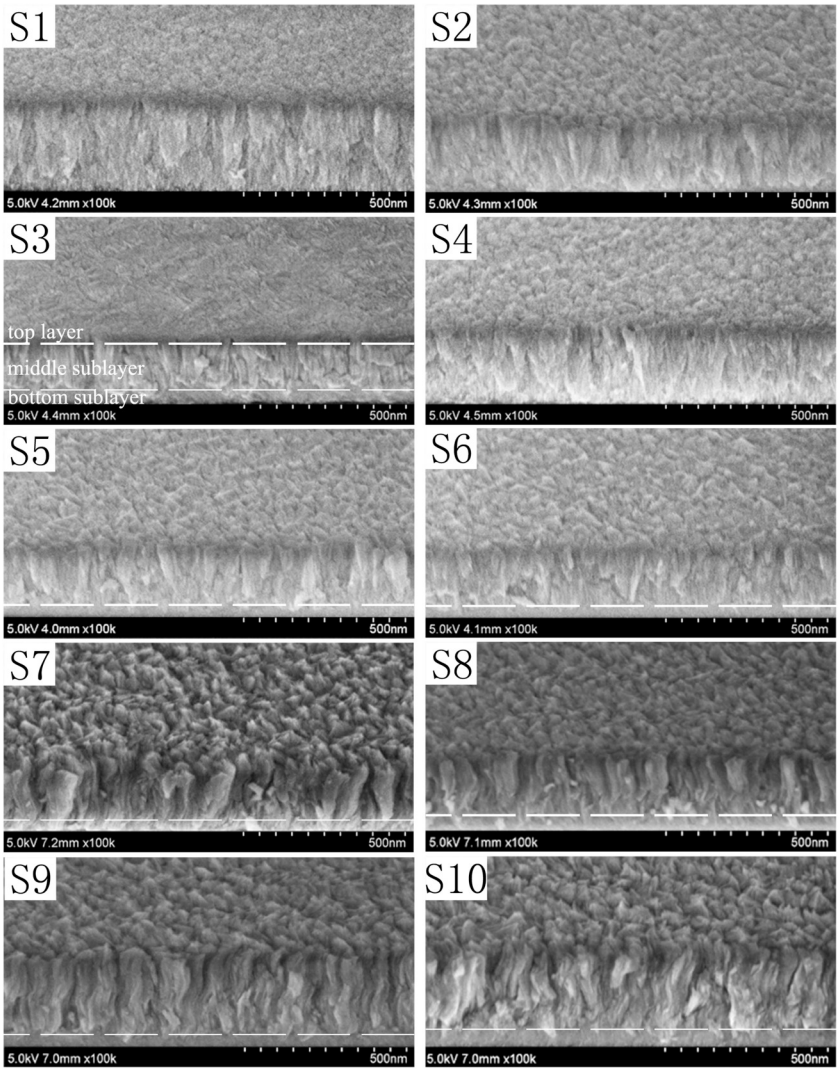

Fig. 4. Cross-sectional SEM images of HfO_2 samples.

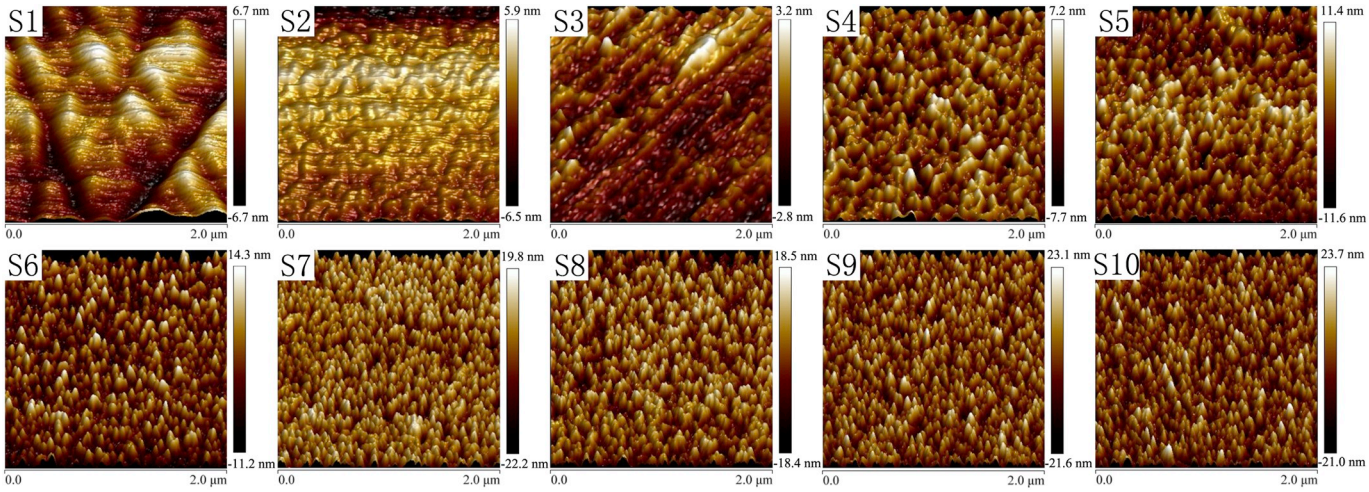

Fig. 5. Surface AFM images of the HfO_2 samples.

detected in the other samples. The Ar content maybe one of the reasons for the additional UV absorption in the film [29].

4. Discussion

For UV laser applications, the most important requirement is low loss, which is dominated by absorption and scattering [4,18,31,32]. Absorption loss is mainly due to impurities and defects. Scattering loss arises from the structure irregularities at the interface and in the bulk. According to nucleation formation theory, the molecular kinetic energy and the deposition conditions are the two main factors that determine the film microstructure and properties [37]. For PIAD techniques, the substrate temperature and bias voltage of the APS plasma will directly influence the kinetic energy of the deposited molecules, whereas the vacuum will also influence the motion of deposited molecules by collision with evaporated molecules [28,31,32,46]. In addition, O_2 can prevent oxygen deficiencies in the HfO_2 film and then reduce the absorption of HfO_2 film. In the following, the influence of four deposition parameters on the optical and structural properties of HfO_2 film was investigated in detail.

4.1. Influence of the APS bias voltage

As presented in Fig. 6a), the refractive index at the wavelength of 250 nm increased gradually when the bias voltage increased from 90 V to 150 V. At the same time, it can be seen from Fig. 6c) that, after storage in atmospheric conditions for three months, samples S2-S5 exhibited a redshift of transmission spectrum, which was an indication of the presence of void structure in the film. It indicated that, even though the film became denser when bias voltage increased, there are still void in the film. Seen from Table 2, the refractive index inhomogeneity was negative when the APS bias voltage was less than or equal to 120 V, while it became positive when the APS bias voltage was 150 V. The sharp variation of the refractive index inhomogeneity with bias voltage indicated that APS bias voltage has a significant influence on the microstructure of HfO_2 films. Importantly, this variation can be further verified by the variation of microstructure with bias voltage in the later. From Fig. 6b), the optical band gap decreased gradually when the bias voltage increased from 90 V to 150 V. It can be explained by the decrease of O/Hf atomic ratio in the HfO_2 films with the increase of bias voltage obtained from the EDX results in Table 2. In addition, the presence of Ar content was also a reason for higher absorption in sample S3 [28].

As shown in Fig. 3, most of the HfO_2 films mainly contained (020) and (021) crystal plane when the bias voltage was less than or equal to 120 V(samples S1, S2, S4), while the HfO_2 films contained only (002) and (−111) crystal plane instead of (020) and (021) crystal plane when the bias voltage was 150 V (sample S3). Sample S5 was a special case. It simultaneously contained (020), (021) and (002) crystal plane. Fig. 6d) presented the crystalline sizes of (020) crystal plane for samples S1, S2, S4 and S5 and (002) crystal plane for samples S3 and S5. As shown in Fig. 6d), the crystalline size of HfO_2 film increased gradually with the increase of APS bias voltage. Seen from Fig. 4, the cross-sectional structure of most HfO_2 films exhibited a uniform arrangement of crystalline columnar in both film growth direction and its vertical direction, when the bias voltage was less than or equal to 120 V(samples S1, S2, S4). At the same time, the boundary of crystal grain was also very faint. However both the size and arrangement of the crystal columnar changed drastically along the film growth direction when the bias voltage was 150 V (sample S3). The cross-sectional of sample S5 can be divided into a thin transition sublayer near the substrate and a top sublayer contained large crystalline columnar along the film growth direction. From the AFM results of S1-S5 in Fig. 5, the significant influence of APS bias voltage on the surface morphology of HfO_2 film was obvious. The RMS value became larger when the APS bias voltage increased from 90 V to 120 V, and then decreased quickly when the APS bias voltage was 150 V.

From the above XRD and SEM results, it can be seen that the variation of cross-sectional structure with APS bias voltage was very similar to that of crystal orientations in total. At the same time, from the above SEM and AFM results, it can be found that, the surface morphology from AFM measurement was amazingly consistent with that of SEM measurement. More importantly, combining the variation of optical and structural properties with APS bias voltage, it can be concluded that the variation of crystal orientation and cross-sectional structure with bias voltage can not only explain the variation of refractive index, but also the variation of the refractive index inhomogeneity with APS bias voltage. It provided a clue for fabricating homogeneous HfO_2 films by PIAD [29].

In general, Preferential crystalline orientations mainly depend on ad-molecules energy [29], substrate temperature, and surface energy of crystallite with different orientations [50]. The increase of kinetic energy of the assisted plasma/ions with the increase of bias voltage will directly increase the ad-molecules energy and may make the deposition condition transferred from zone T to zone II according to the structure zone model of Messier [48] and Thornton [49]. So it indicated that film growth of sample S1, S2, and S4 were located in zone T, while film growth of sample S3 was located in zone II, and film growth of sample S5 was located between zone T and II. It determined the variation of crystal orientation, cross-sectional structure and surface morphology

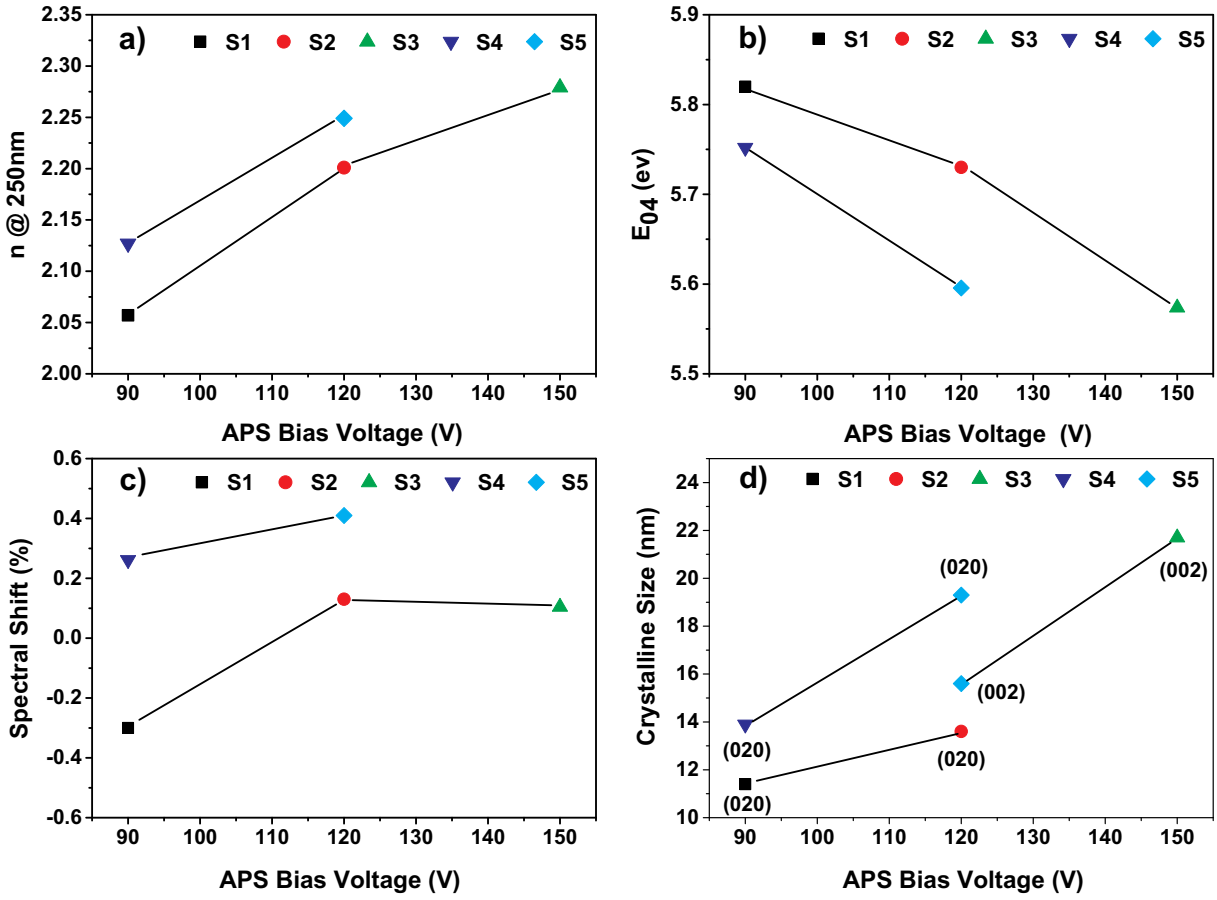

Fig. 6. Refractive index, E04, spectral shift, and crystalline size vs. APS bias voltage.

with APS bias voltage.

4.2. Influence of substrate temperature

From Fig. 7a) and b), the HfO_2 films (Sample S6, S5, S7) have nearly the same refractive index at the wavelength of 250 nm and optical bandgap when the substrate temperature was less than or equal to 250 ˚C. The refractive index at 250 nm increased slightly and optical bandgap decreased slightly when the substrate temperature increased to 300 ˚C (Sample S8). At the same time, it can be seen from Fig. 7c) that, the transmission spectra of all samples S5-S8 shift to longer wavelengths after storage in atmospheric conditions, which was an indication of the presence of void structure in the film. However, it can be seen from Table 2 that, the negative degree of refractive index inhomogeneity became more severe when the substrate temperature increased from 150 ˚C (sample S6) to 250 ˚C (sample S7), while the refractive index became homogenous when substrate temperature further increased to 300 ˚C (sample S8). The sharp variation of the refractive index inhomogeneity when substrate temperature increased from 250 ˚C to 300 ˚C indicated the corresponding change of microstructure in HfO_2 films, which can be verified in the following.

From Fig. 3, the variation of crystalline orientations in HfO_2 films with substrate temperature can be divided into three kinds. For the (020) and (021) crystal plane, the diffraction intensities increased slightly when substrate temperature increased from 150 ˚C (sample S6) to 200 ˚C (sample S5). However these two orientations disappeared when substrate temperatures were 250 ˚C (samples S7) and 300 ˚C (samples S8). For the (002) crystal plane, it can be hardly detected in sample S6 and begin to appear in sample S5. Its intensity increased in sample S7 and then decreased in sample S8. For the (−111) crystal plane, it could not be detected in samples S6 and S5. However, it appeared in samples S7 and S8, and its intensity increased when the substrate temperature increased from 250 ˚C (sample S7) to 300 ˚C (sample S8). Fig. 7d) presented the crystalline sizes of (020) orientation for samples S6 and S5, and the crystalline sizes of (002) crystal plane for samples S5, S7, and S8. As shown in Fig. 7d), though the crystalline sizes of samples S5-S8 increase gradually with increasing substrate temperature, the absolute increment of crystalline size was relatively small. From Fig. 4, it can be seen that, though both the top morphology and cross-sectional of HfO_2 films were similar when the substrate temperature was less than or equal to 250 ˚C(samples S6, S5, S7), the crystalline grain became more apparent and regular when substrate temperature increased from 150 ˚C to 250 ˚C. When substrate temperature increased from 250 ˚C to 300 ˚C (samples S8), the top morphology of HfO_2 films became more coarse and cross-sectional structure exhibited a significantly sharp change. In addition, there is a thin transition sublayer near the substrate in all four samples. From the AFM results of sample S5-S8 in Fig. 5 and Table 2, it was obvious that, the top morphology of all four sample was similar each other, but the RMS value decreased gradually when substrate temperature increased from 150 ˚C to 250 ˚C and then increased quickly when substrate temperature increased to 300 ˚C.

From the above XRD, SEM and AFM results, it can be seen that the variation of crystal orientations with substrate temperature was a bit different from that of cross-sectional structure, but the variation of top morphology from AFM was amazingly consistent with that from SEM. Combining the variation of the optical and structural properties with substrate temperature, it can be found that the variation of the cross-section with substrate temperature can intuitively explain that of the refractive index with substrate temperature. When the sharp change of

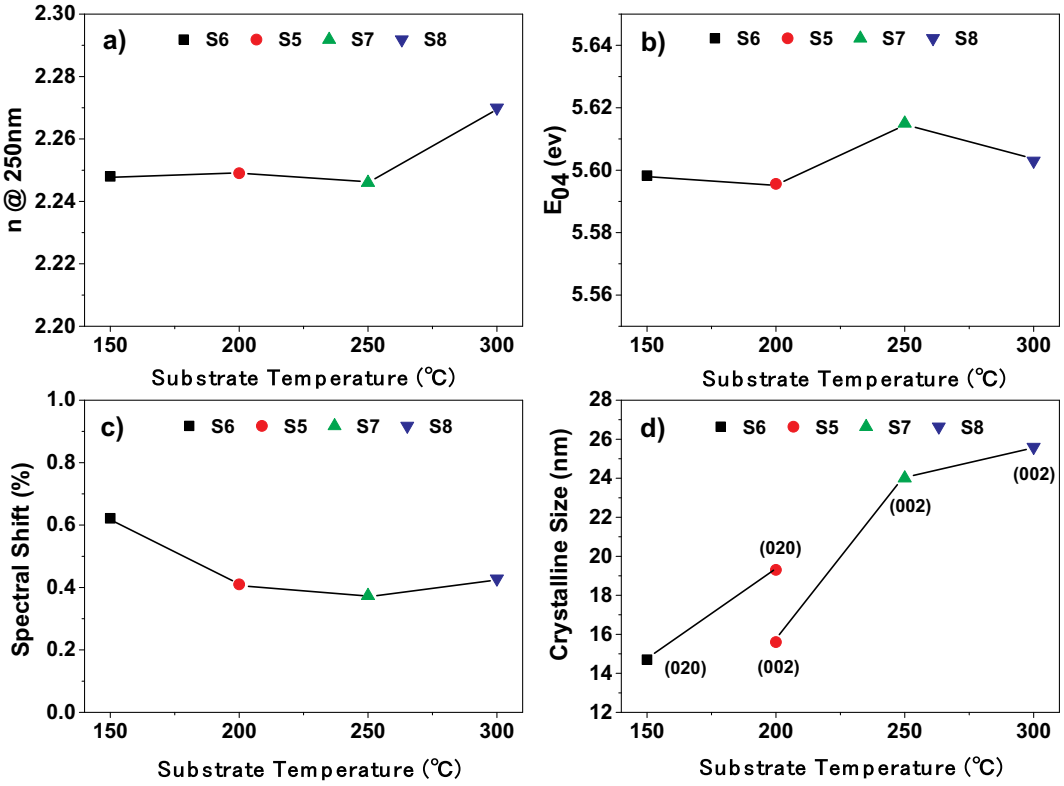

Fig. 7. Refractive index, E_{04}, spectral shift, and crystalline size vs. substrate temperature.

the refractive index inhomogeneity in samples S7 and S8 was considered, the influence of (−111) crystal plane on the microstructure and then on refractive index homogeneity was obvious. As stated in Section 4.1, preferential crystalline orientations mainly depend on ad-molecules energy [30], substrate temperature, and surface energy of crystallite with different orientations [50]. The increase of substrate temperature will directly increase the ad-molecules energy, which may make the deposition condition transferred from zone T to zone II according to the structure zone model of Messier [48] and Thornton [49]. It may be the reason for the transition of preferential orientation from (020) crystal plane in sample S6 and S5 to (−111), (002) and (013) crystal plane in sample S7 and S8.

4.3. Influence of O_2 flow rate in chamber

It should be noted that, though all the samples discussed in this section have been discussed in Section 4.1, the influence of the chamber O_2 flow rate was focused here. As shown in Fig. 8a) and b), the refractive index of HfO_2 films decreased while the optical band gap increased when the chamber O $_2$ flow rate increased from 20 sccm to 30 sccm, regardless of the bias voltage was 90 V or 120 V. Seen from Table 2, the refractive index inhomogeneity of samples S1, S2, S4, and S5 were all negative. However, the variation trend of refractive index inhomogeneity with chamber O_2 flow rate in the investigated range of this paper was not clear. The EDX results showed that the O/Hf atomic ratio increased with the increase of chamber O_2 flow rate, regardless of whether the bias voltage was 90 V or 120 V. It can explain the variation of the optical band gap with the chamber O_2 flow rate.

Seen from Fig. 3, all the HfO_2 films contained (020) and (021) crystal plane regardless of the chamber O_2 flow rate was 20 sccm (sample S4 and sample S5) or 30 sccm (sample S1 and sample S2), while sample S5 contained additional (002) crystal plane. But as shown in Fig. 8d), the crystalline size decreased when the chamber O_2 flow rate increased from 20 sccm to 30 sccm. As discussed in Section 4.1, the crystalline grain in samples S1, S2, and S4 distributed uniform in both the film growth direction and its vertical direction, while the crystalline grain arrangement of sample S5 was obviously not uniform in the film growth direction. In addition, SEM results indicated that the crystalline grain in samples S4 and S5 was obviously larger than that in samples S1 and S2. From AFM measurements, it can be seen that the chamber O_2 flow rate has a significant influence on the surface top morphology of HfO_2 film, and the RMS value decreased significantly when the chamber O_2 flow rate increased from 20 sccm to 30 sccm, regardless of the bias voltage was 90 V or 120 V. Importantly, top morphology from AFM measurements was amazingly consistent with that of SEM measurement.

From the above XRD, SEM, and AFM results, it can be seen that the variation of cross-sectional structure with the chamber O_2 flow rate was well similar to that of crystal orientations in total, and the surface morphology from AFM measurement was amazingly consistent with that of SEM measurement. More importantly, the variation of microstructure with the APS O_2 flow rate can well correlate to that of optical properties. According to film formation theory, an increase of the chamber O_2 flow rate will directly decrease the vacuum of the coating chamber and then decrease the kinetic energy of deposited particles by collisions with evaporated molecules. It resulted in looser microstructures and a lower refraction index of the HfO_2 film.

4.4. Influence of O_2 flow rate in the APS

As presented in Fig. 9a) and b), when the APS O_2 flow rate increased from 20 sccm to 25 sccm, the refractive index of HfO_2 film also increased, while the optical band gap decreased. When the APS O_2 flow rate further increased from 25 sccm to 30 sccm, the refractive index of HfO_2 film decreased, while the optical band gap increased. As presented in Table 2, all samples S9, S5 and S10 exhibited negative refractive index inhomogeneity and the O/Hf atomic ratio decreased when the APS O_2 flow rate increased from 20 sccm to 25 sccm and then increased when the APS O_2 flow rate further increased to 30 sccm. The variation of the O/Hf atomic ratio with the APS O_2 flow rate explained that of the

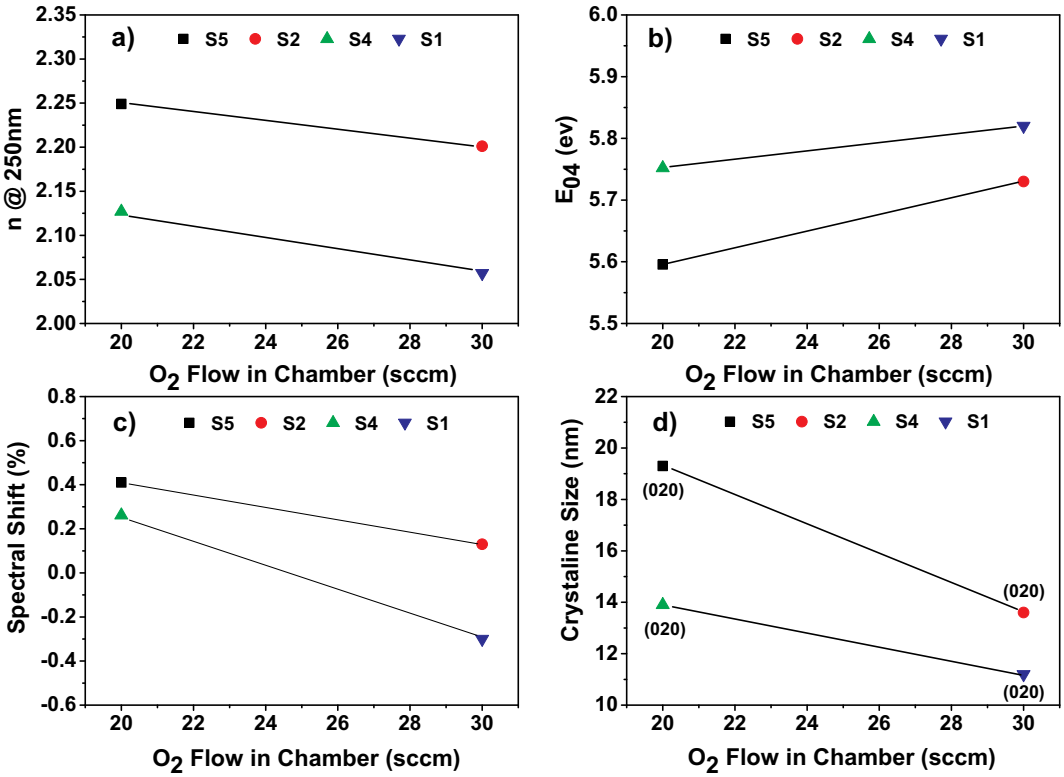

Fig. 8. Refractive index, E_{04}, spectral shift, and crystalline size vs. O_2 flow rate in the chamber.

optical band gap.

As shown in Fig. 3, all samples S9, S5 and S10 mainly contained (020) and (021) crystal plane, while sample S5 contained an additional (002) crystal plane. As presented in Fig. 9d), the grain size of the HfO_2 film increased when the APS O_2 flow rate increased from 20 sccm to 25 sccm and then decreased when the APS O_2 flow rate further

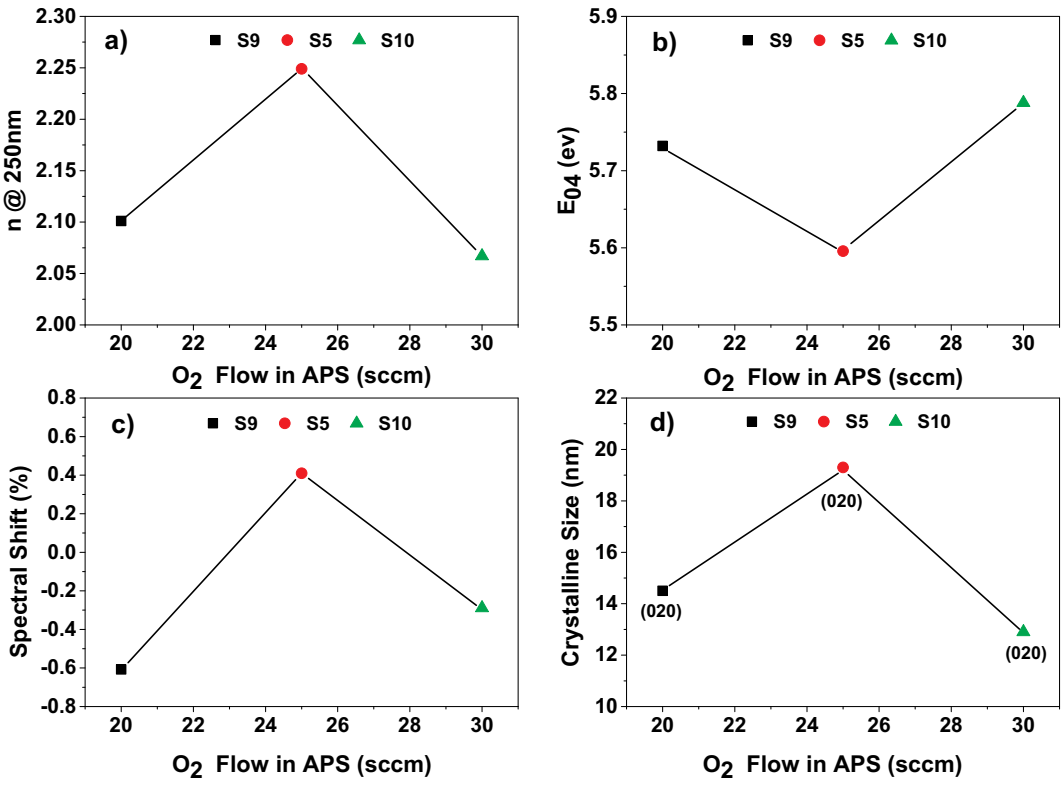

Fig. 9. Refractive index, E_{04}, spectral shift, and crystalline size vs. O_2 flow rate in the APS.

increased to 30 sccm. From Fig. 4, it can be seen that, the cross-sectional structure of all samples S9, S5 and S10 were similar and has an obvious transition sublayer near the substrate and large crystalline columnar along the film growth direction. The top morphology of all three samples was also similar. But it seems that the top morphology of sample S5 was more smooth than sample S9 and S10. The top morphology from AFM measurements was consistent with that of SEM measurement. The RMS decreased significantly when the APS O_2 flow rate increased from 20 sccm to 25 sccm and then increased significantly when the APS O_2 flow rate further increased to 30 sccm.

From the above results, it can be seen that the variation of optical properties with the APS O_2 flow rate was well correlated to that of microstructure. Importantly, the influence of the APS O_2 flow rate on the microstructure and optical constants of HfO_2 film was not monotonous when the APS O_2 flow rate was in the range from 20 sccm to 30 sccm, which indicated that the APS O_2 flow rate was a very sensitive process parameter. In general, the increase of the APS O_2 flow rate not only changed the partial pressure of O_2 and the vacuum of chamber, but also changed the Ar/O ratio and kinetic energy of assisted plasma. When the APS O_2 flow rate increased from 25 sccm to 30 sccm, the comprehensive effects were to decrease the vacuum of the coating chamber and the kinetic energy of the evaporated particles, which induced a looser microstructure, smaller crystalline size, and lower refractive index. But the optical band gap increased due to the increase of O_2 atoms/ions partial pressure. When the APS O_2 flow rate increased from 20 sccm to 25 sccm, it seems that the change of Ar/O ratio and kinetic energy of assisted plasma played a more important role than that of chamber vacuum and O_2 partial pressure, which induced a denser structure, larger crystalline size, higher refractive index and absorption.

4.5. Comparison with literature data

Fig. 10 presented the optical constants at the wavelength of 250 nm of the selected samples (S2 and S5) and the corresponding data in the literature [6,15,18,28,31]. Omitting the influence of film thickness and refractive index inhomogeneity, it was obvious that the refractive indices of samples S2 and S5 were similar to that of the selected literature. But the extinction coefficients of samples S2 and S5 are nearly the lowest in all the compared data. As shown in Table 2, the surface roughness values of samples S2 and S5 were 1.57 nm and 3.18 nm, respectively. These values are also relatively low when compared to that of the selected literature.

Using HfO_2 film with the property of sample S5 as a high-index material and SiO_2 film as a low-index material, a 248 nm HR with an incident angle of 45° was designed and fabricated. This HR sample adopted a standard quarter-wave design contained 32 layers in total. Fig. 11 presented the measured reflection spectrum. The reflectivity

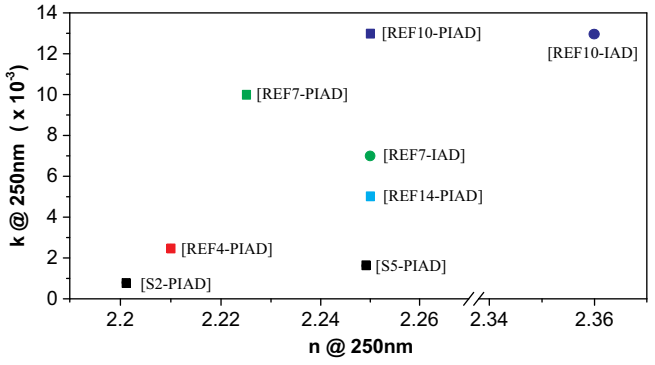

Fig. 10. Extinction coefficients vs. refractive index at 250 nm. S2-PIAD and S5-PIAD originate from the present study.
The other data are taken from the literature [6,15,18,28].

was close to 99.5% at 248 nm, which confirmed the excellent UV optical properties of sample S5 in this study.

5. Conclusion

HfO_2 films were prepared by varying four process parameters of PIAD, including the APS bias voltage, the substrate temperature, the chamber O_2 flow rate and the APS O_2 flow rate. The optical and structural properties of the deposited HfO_2 films, including the refractive index, extinction coefficient, optical band gap, spectral shift, crystalline state, surface morphology, SEM cross-section, and O/Hf atomic ratio, were systematically characterized. The specific influences of different process parameters on the properties of the HfO_2 films were evaluated in detail by investigating the correlations between the optical and structural properties. The obtained results favor a more detailed understanding of the specific roles or influence mechanisms of the four different parameters in the elementary deposition processes of HfO_2 films deposited by PIAD.

- As the APS bias voltage increased from 90 V to 120 V, the crystallinity of the HfO_2 films gradually changed from a weak monoclinic phase to a strong monoclinic phase, which mainly consisted of (020) and (021) crystal plane. As the bias voltage further increased to 150 V, the (−111) and (002) crystal plane became the preferred growth orientations, while the (020) and (021) crystal plane became limited growth orientations. As a result, the crystalline size, refractive index, and absorption of the HfO_2 films gradually increased with increasing bias voltage. In addition, the refractive index inhomogeneity was negative when the bias voltage was less than or equal to 120 V and became positive when the bias voltage was 150 V.
- As the substrate temperature increased from 150 °C to 300 °C, the crystallinity of the HfO_2 films gradually changed from a weak monoclinic phase to a strong monoclinic phase, accompanied by a significant increase of the crystalline size and variation of the main orientation. As a result, the refractive index of the HfO_2 films gradually increased with increasing substrate temperature, while the absorption was nearly unchanged. The refractive index inhomogeneity was negative when the substrate temperature was less than or equal to 250 °C and became positive when the substrate temperature was 300 °C.
- As the chamber O_2 flow rate increased from 20 sccm to 30 sccm, the crystalline size, refractive index, and absorption of the HfO_2 films also decreased. However, the decrease was relatively small.
- As the APS O_2 flow rate increased from 20 sccm to 30 sccm, the influence on the optical and structural properties was not monotonous and more complex than that of the chamber O_2 flow rate.
- By comparing the refractive index and extinction coefficients at the wavelength of 250 nm with those in the literature, it can be concluded that the optimized HfO_2 samples have been obtained with very low UV absorption, which will facilitate the production of UV coatings with high laser damage resistance and high spectrum performance.

Author contribution statement

1. Wenyuan Deng contributed to design the experiments, perform the data analyses and wrote the manuscript.
2. Chunshui Jin contributed to conceiv the experiments.
3. Chun Li and Shun Yao contributed significantly to the experiments and analysis.
4. Bo Yu performed the data analyses and wrote the manuscript;
5. Yu Liu helped performing AFM measurement.

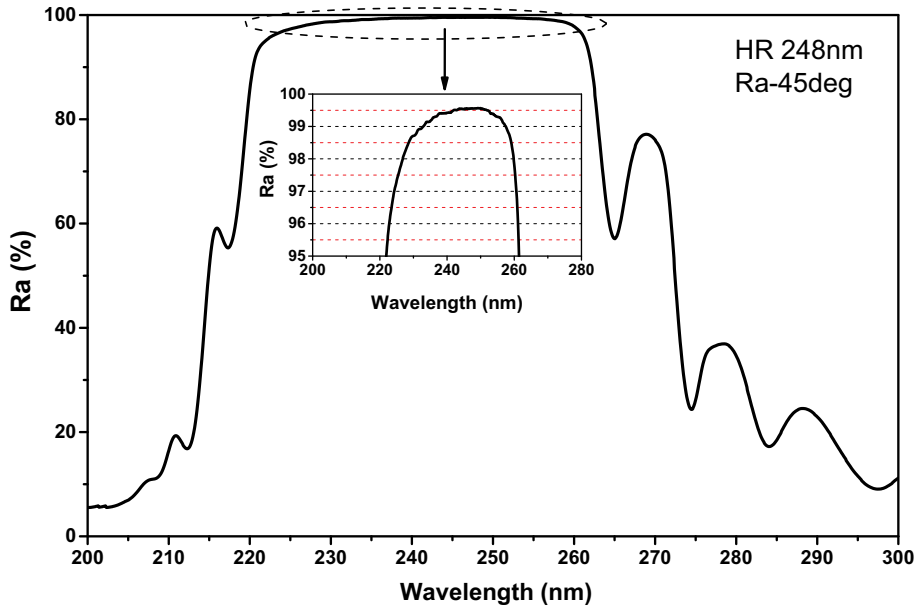

Fig. 11. The reflection spectrum of the HR 248 nm sample with an incident angle of 45°. The insert curve is an enlarged display.

Declaration of competing interest

The authors declare that they have no known competing financial interests or personal relationships that could have appeared to influence the work reported in this paper.

Acknowledgments

This research was financially supported by the Science and Technology Development Project of Jilin Province (No. 20180101284JC), National Natural Science Foundation of China (NSFC) (Nos. 61178020, 61505202, and 21603211), and Jilin Province Yong Talent Fund Projects (No. 20180520156JH).

References

[1] A. Gatto, R. Thielsch, J. Heber, N. Kaiser, D. Ristau, S. Günster, J. Kohlhaas, M. Marsi, M. Trovò, R. Walker, D. Garzella, M.E. Couprie, P. Torchio, M. Alvisi, C. Amra, High-performance deep-ultraviolet optics for free-electron lasers, Appl. Opt. 41 (16) (2002) 3236–3241.
[2] J.B. Oliver, P. Kupinski, A.L. Rigatti, A.W. Schmid, J.C. Lambropoulos, S. Papernov, A. Kozlov, J. Spaulding, D. Sadowski, Z.R. Chrzan, R.D. Hand, D.R. Gibson, I. Brinkley, F. Placido, Large-aperture plasma-assisted deposition of inertial confinement fusion laser coatings, Appl. Opt. 50 (1) (2011) 19–26.
[3] James B. Oliver, Evaporated HfO_2/SiO_2 Optical Coatings and Modifications for High-power Laser Applications, D University of Rochester, 2012.
[4] R.G. Safin, I.S. Ganutdinov, R.S. Sabirov, M.Kh. Azamatov, Solar-blind filter for the ultraviolet region, J. Opt. Technol. 74 (3) (2007) 208–210.
[5] Zhiyuan Wang, Xiaoxin Wang, Jifeng Liu, Design of nanophotonic, hot-electron solar-blind ultraviolet detectors with a metal-oxide-semiconductor structure, J. Opt. 16 (2014) 125010.
[6] Samuel F. Pellicori, Carol L. Martinez, UV optical properties of thin film oxide layers deposited by different processes, Appl. Opt. 50 (28) (2011) 5559–5566.
[7] Jue Wang, Gary A. Hart, Jean Francois Oudard, Leonard Wamboldt, Brian P. Roy, HfO_2/SiO_2 multilayer based reflective and transmissive optics from the IR to the UV, Proc. SPIE 9822 (2016) 98220Z.
[8] S. Jena, R.B. Tokas, S. Tripathi, K.D. Rao, D.V. Udupa, S. Thakur, N.K. Sahoo, Influence of oxygen partial pressure on microstructure, optical properties, residual stress and laser induced damage threshold of amorphous HfO_2 thin films, J. Alloys Compd. 771 (2019) 373–381.
[9] S. Papernov, M.D. Brunsman, J.B. Oliver, B.N. Hoffman, A.A. Kozlov, S.G. Demos, A. Shvydky, F.H.M. Cavlcante, L. Yang, C.S. Menoni, B. Roshanzadeh, S.T.P. Boyd, L.A. Emmert, W. Rudolph, Optical properties of oxygen vacancies in HfO_2 thin films studied by absorption and luminescence spectroscopy, Opt. Express 26 (2018) 17608–17623.
[10] J. Wang, M.J. Cangemi, C.J. Chinhong, et al., Characterization of reactive plasma ion assisted HfO_2 films for low loss optical coatings in the DUV and MWIR, Proc. SPIE 10181 (2017) 101810P.
[11] Rogéria R. Goncalves, G. Carturan, M. Montagna, et al., Erbium-activated HfO_2-based waveguides for photonics, Opt. Mater. 25 (2) (2004) 131–139.
[12] M.P. Nielsen, A. Ashfar, K. Cadien, et al., Plasmonic materials for metal–insulator–semiconductor–insulator–metal nanoplasmonic waveguides on silicon-on-insulator platform, Opt. Mater. 36 (2) (2013) 294–298.
[13] T.R. Jensen, J. Warren, R.L. Johnson Jr., Ion-assisted deposition of moisture-stable hafnium oxide films for ultraviolet applications, Appl. Opt. 41 (2002) 3205–3210.
[14] H. Jiao, X. Cheng, J. Lu, G. Bao, Y. Liu, B. Ma, P. He, Z. Wang, Effects of substrate temperatures on the structure and properties of hafnium dioxide films, Appl. Opt. 50 (2011) 309–315.
[15] R. Thielsch, A. Gatto, J. Herber, N. Kaiser, A comparative study of the UV optical and structural properties of SiO_2, Al_2O_3, and HfO_2 single layers deposited by reactive evaporation, ion-assisted deposition and plasma ion-assisted deposition, Thin Solid Films 410 (2002) 86–93.
[16] C.J. Stolz, L.M. Sheehan, M.K. von Gunten, R.P. Bevis, D.J. Smith, Advantages of evaporation of hafnium in a reactive environment for manufacture of high-damage threshold multilayer coatings by electron beam evaporation, Proc. SPIE 3738 (1999) 318–324.
[17] B. Andre, L. Poupinet, G. Ravel, Evaporation and ion assisted deposition of HfO_2 coatings: some key points for high power laser applications, J. Vac. Sci. Technol. 18 (5) (2000) 2372–2377.
[18] Philippe Torchio, Alexandre Gatto, Marco Alvisi, Ge rard Albrand, Norbert Kaiser, Claude Amra, High-reflectivity HfO_2/SiO_2 ultraviolet mirrors, Appl. Opt. 41 (16) (2002) 3256–3261.
[19] M. Alvisi, M. Di Giulio, S.G. Marrone, M.R. Perrone, M.L. Protopapa, A. Valentini, L. Vasanelli, HfO_2 films with high laser damage threshold, Thin Solid Films 410 (1) (2002) 86–93.
[20] D. Zhang, S. Fan, Y. Zhao, W. Gao, J. Shao, R. Fan, Y. Wang, Z. Fan, High laser-induced damage threshold HfO_2 films prepared by ion-assisted electron beam evaporation, Appl. Surf. Sci. 243 (1–4) (2005) 232–237.
[21] G. He, X. Chen, Z. Sun, Interface engineering and chemistry of Hf-based high-k dielectrics on III–V substrates, Surf. Sci. Rep. 68 (1) (2013) 68–107.
[22] Gang He, Bin Deng, Hanshuang Chen, Xiaoshuang Chen, Jianguo Lv, Yongqing Ma, Zhaoqi Sun, Effect of dimethyllaluminumhydride -derived aluminum oxynitride passivation layer on the interface chemistry and band alignment of HfTiO-InGaAs gate stacks, APL Mater. 1 (2013) 012104.
[23] Gang He, Liu Jiangwei, Chen Hanshuang, M. Liu, Sun Zhaoqi, Chen Xiaoshuang, Liu Mao, Zhang Lide, Interface control and modification of band alignment and electrical properties of HfTiO/GaAs gate stacks by nitrogen incorporation, J. Mater. Chem. C 2 (27) (2014) 5299–5308.
[24] J.W. Zhang, Gang He, L. Zhou, Chen Hanshuang, X.S. Chen, X.F. Chen, B. Deng, J.G. Lv, Z.Q. Sun, Microstructure optimization and optical and interfacial properties modulation of sputtering-derived HfO_2 thin films by TiO_2 incorporation, J. Alloys Compd. 611 (2014) 253 J. Alloys Comp.
[25] Gang He, Juan Gao, Hanshuang Chen, Jingbiao Cui, Zhaoqi Sun, Xiaoshuang Chen, Modulating the interface quality and electrical properties of HfTiO/InGaAs gate stack by atomic-layer-deposition-derived Al_2O_3 passivation layer, ACS Appl. Mater. Interfaces 6 (24) (2014) 22013–22025.
[26] Z. Jinlong, C. Xinbin, W. Zhanshan, J. Hongfei, D. Tao, HfO_2/SiO_2 chirped mirrors manufactured by electron beam evaporation, Appl. Opt. 50 (9) (2011) C388–C391.
[27] R. Thielsch, T. Feigl, N. Kaiser, S. Martin, S. Scaglione, F. Sarto, M. Alvisi, A. Rizzo, Comparison of the optical properties and UV radiation resistance of HfO_2 single layers deposited by reactive evaporation, IAD, and PIAD, Proc. SPIE 3902 (2000)

182–193.
[28] Meiping Zhu, Kui Yi, Detlef Arhilger, Hongji Qi, Jianda Shao, Effect of Advanced Plasma Source bias voltage on properties of HfO_2 films prepared by plasma ion assisted electron evaporation from metal, Thin Solid Films 540 (2013) 17–22.
[29] M. Alvisi, S. Scaglione, S. Martelli, A. Rizzo, L. Vasanelli, Structural and optical modification in hafnium oxide thin films related to the momentum parameter transferred by ion beam assistance, Thin Solid Films 354 (1999) 19–23.
[30] O. Stenzel, S. Wilbrandt, N. Kaiser, Optical characterization of high index metal oxide films for UV-VIS applications prepared by Plasma Ion Assisted Deposition, Proc. SPIE 9627 (2015) 962709.
[31] O. Stenzel, S. Wilbrandt, S. Yulin, N. Kaiser, M. Held, A. Tünnermann, J. Biskupek, U. Kaiser, Plasma ion assisted deposition of hafnium dioxide using argon and xenon as process gases, Opt. Mater. Express 1 (2011) 278–292.
[32] J. Wang, R.L. Maier, H. Schreiber, Crystal phase transition of HfO_2 films evaporated by plasma-ion-assisted deposition, Appl. Opt. Suppl. 47 (2008) C189–C192.
[33] Laurent Gallais, Jérémie Capoulade, Jean-Yves Natoli, Mireille Commandré, Michel Cathelinaud, Cian Koc, Michel Lequime, Laser damage resistance of hafnia thin films deposited by electron beam deposition, reactive low voltage ion plating, and dual ion beam sputter, Appl. Opt. 47 (13) (2008) C107–C113.
[34] D. Zhang, P. Fan, C. Wang, X. Cai, G. Liang, J. Shao, Z. Fan, Properties of HfO_2 thin films prepared by dual ion-beam reactive sputtering, Opt. Laser Technol. 41 (2009) 820–822.
[35] C.J. Stolz, F.Y. Genin, M.R. Kozlowski, D. Long, R. Lalazari, Z. Wu, P.-K. Kuo, Influence of microstructure on laser damage threshold of IBS coatings, Proc. SPIE 2714 (1996) 351–359.
[36] O. Stenzel, S. Wilbrandt, M. Schürmann, N. Kaiser, H. Ehlers, M. Mende, D. Ristau, S. Bruns, M. Vergöhl, M. Stolze, M. Held, H. Niederwald, T. Koch, W. Riggers, P. Burdack, G. Mark, R. Schäfer, S. Mewes, M. Bischoff, M. Arntzen, F. Eisenkrämer, M. Lappschies, S. Jakobs, S. Koch, B. Baumgarten, A. Tünnermann, Mixed oxide coatings for optics, Appl. Opt. 50 (9) (2011) C69–C74.
[37] Michal Mazur, Torsten Howind, Des Gibson, Danuta Kaczmarek, Jerzy Morgiel, Damian Wojcieszak, Wenzhong Zhu, Piotr Mazur, Modification of various properties of HfO_2 thin films obtained by changing magnetron sputtering conditions, Surf. Coat. Technol. 320 (2017) 426–431.
[38] S. Jena, R.B. Tokas, J.S. Misal, K.D. Rao, D.V. Udupa, S. Thakur, N.K. Sahoo, Effect of O_2/Ar gas flow ratio on the optical properties and mechanical stress of sputtered HfO_2 thin films, Thin Solid Films 592 (2015) 135–142.
[39] M. Vargas, N.R. Murphy, C.V. Ramana, Structure and optical properties of nanocrystalline hafnium oxide thin films, Opt. Mater. 37 (2014) 621–628.
[40] K. Ettrich, H. Blaschke, E. Welsch, P. Thomsen-Schmidt, D. Schafer, UV-laser investigation of dielectric thin films, Proc. SPIE 2714 (1996) 426–439.
[41] A.V. Tikhonravov, M.K. Trubetskov, OptiChar Software, http://www.optilayer.com.
[42] A.V. Tikhonravov, M.K. Trubetskov, T.V. Amotchkina, G. DeBell, V. Pervak, A.K. Sytchkova, M.L. Grilli, D. Ristau, Optical parameters of oxide films typically used in optical coating production, Appl. Opt. 50 (9) (2011) C75–C85.
[43] O. Stenzel, S. Wilbrandt, N. Kaiser, M. Vinnichenko, F. Munnik, A. Kolitsch, A. Chuvilin, U. Kaiser, J. Ebert, S. Jakobs, A. Kaless, S. Wüthrich, O. Treichel, B. Wunderlich, M. Bitzer, M. Grössl, The correlation between mechanical stress, thermal shift and refractive index in HfO_2, Nb_2O_5, Ta_2O_5 and SiO_2 layers and its relation to the layer porosity, Thin Solid Films 517 (21) (2009) 6058–6068.
[44] G. Abromavicius, R. Buzelis, R. Drazdys, D. Perednis, A. Skrebutenas, Optimization of HfO_2, Al_2O_3 and SiO_2 deposition leading to advanced UV optical coatings with low extinction, Proc. SPIE, 6596 2007 (65961N).
[45] J.P. Lehan, Y. Mao, B.G. Bovard, H.A. Macleod, Optical and microstructural properties of hafnium dioxide thin films, Thin Solid Films 203 (1991) 227–250.
[46] N. Kaiser, Review of the fundamentals of thin-film growth, Appl. Opt. 41 (2002) 3053–3060.
[47] Daniel Franta, Ivan Ohlídal, David Nečas, František Vižd'a, Ondřej Caha, Martin Hasoň, Pavel Pokorný, Optical characterization of HfO_2 thin films, Thin Solid Films 519 (2011) 6085–6091.
[48] R. Messier, A.P. Giri, R.A. Roy, Revised structure zone model for thin film physical structure, J. Vac. Sci. Technol. A 2 (2) (1984) 500–503.
[49] J.A. Thornton, The microstructure of sputter-deposited coatings, J. Vac. Sci. Technol. A4 (6) (1986) 3059.
[50] L. Pereira, P. Barquinha, E. Fortunato, R. Martins, Influence of the oxygen/argon ratio on the properties of sputtered hafnium oxide, Mater. Sci. Eng. B 118 (2005) 210–213.